Arraying Techniques for the Galileo S-Band Mission, Part II - Complex Symbol Combining*

S. Million, 13. Shah and S. Hinedi
Jet **Propulsion Laboratory**
California Institute **of Technology**
4800 **Oak Grow Dr., MS 238-343**
Pasadena, CA 91109

February **7, 1994**

Abstract

Antenna arraying is becoming an increasingly popular technique to enhance the quality of signals received from distant transmitters. in principle, arraying is a simple concept that increases signal-to-noise (SNR) ratio by combi ning waveforms with identical signal sources and independent noise sources. in practice, however, the combining algorithm has significant impact on the gain or actual increase in SNR achieved.

The second part of this two part article describes and evaluates the gain that can be achieved by implementing the Complex Symbol Combining (CSC) algorithm. Results obtained here are then compared to the Full-Spectrum Combining (FSC) algorithm, which was presented in part 1. Specifically, for the following arrays - two 70-m antennas, one 70-m and one 34-m antennas, one 70-m and two 34-m antennas, and one 70-m and three 34-m antennas - it is shown that FSC has less degradation than CSC when the subcarrier and symbol window-loop bandwidth product is above 3,0, 10.0, 8.5, and 8.2 mHz at a symbol rate of 200 sym/see, and above 1.2, 4.5, 4.0, and 3.5 mHz at a symbol rate of 400 sym/see, respect, vely. Moreover, for an array of four 34-m antennas, FSC has less degradation than CSC when the subcarrier and symbol window-loop bandwidth product is above 0,32 mHz at the symbol rate of 50 sym/see, and above 0.8 mHz at the symbol rate of 25 sym/sec.

* The work described in this paper was carried out by the Jet 1 'ropulsion Laboratory, California institute of Technology, under a contract with the National Aeronautics and Spare Administration.

1 Introduction

In deep space communications, combining signals from multiple antennas is commonly referred to as arraying. Arraying is particular] y attractive when the communi cation links arc operating near threshold. Consider, for instance, the Galileo spacecraft which duc to a malfunction high gain antenna must rel y on its low gain S-band (2.2 to 2.3 GI 1 z) antenna for data communication. in order to improve its link margin and maximize data return, the Galileo S-band mission will employ arraying, and other techniques such as data compression and suppressed carriers. This article describes the Complex Symbol Combining (CSC) arraying techni quc which has been made possible by the advent of all-digital receivers in NA SA's deep space communications network [1]. This is an attracti vc arraying option because it requires little modification to exi sting systems. The CSC techni quc is, subsequentl y, compared to the l"ull-Spectrum Combining (FSC) technique, described in part I of this article, for the following five arrays: two 70-m antennas; one 70-m and one 34-m antenna; one 70-m and two 34-m antennas; one 70-m and three 34-m antennas; and four 34-m antennas.

in CSC, depicted in Fig. 1 (a), the received RF signal at each antenna is first open-loop downconverted to 1 F; it, in turn, is open-loop downconverted to baseband using a complex IF reference. The IF in-phase (1) and quadrature (C)) references arc tuned to the predicted IF carrier frequency. The resulting complex baseband signal, centered at the carrier predict error, is used for subcarrier tracking and symbol synchronization which can bc accomplished using either the 1 arm of the carrier alone or both t] ic 1 and Q arms. The latter requires more complexit y but resul ts in an improved performan cc as one would expect. A ftcr subcarrier demodulation, the signal is input to a pair of matched filters which output soft-quantized complex symbols that modulate a tone with frequency equal to the carrier predict error. Since there arc two channels in the down conversion process (carrier 1 and carrier Q), the symbols at the matched filter output modulate quadrature tones and can bc viewed as complex symbols. The complex symbols from multiple antennas arc then transmitted to

a central location, aligned and combined at baseband, and demodulated using a baseband Costas loop. The CSC output is a single real combined symbol stream. The combiner for CSC is shown in Fig. 1 (b) and discussed in the section on CSC performance.

The kcy difference between CSC and FSC is the order of carrier-phase alignment between the antennas. Whereas in FSC, carrier-plmsc alignment precedes subcarrier demodulation, symbol synchronization, and matched filtering, in CSC, it follows. In both cases, the carrier phases are aligned and the signals arc combined prior to carrier phase tracking and demodul ation. As a result, for an array of two 70-m antennas, the effective P/N_0 at the input to the subcarrier and symbol loops in (XC is about 6 dB lower than FSC. Three of the 6 dBs arc duc to the signals in CSC being combined after the subcarrier and symbol loops; the remaining 3 dB result from subcarrier and symbol synchronization that arc performed without carrier lock. Assuming the carrier is locked, the effective P/N_0 at the input to the subcarrier and symbol loops in CSC is about 3 d] 3 lower than FSC. Another kcy difference between CSC and FSC arises when arraying a 70-m and 34-m antenna. in the Galileo case, the signal is so weak that it is harder for a stand alone 34-m antenna to lock to the signal than a stand-alone! 70-m antenna. Consequently, when implementing CSC between the two, the 70-m antenna needs to enable the 34-m antenna in tracking the subcarrier and symbols. When they are located within a fcw miles of each other, the 70-m antenna can transmit subcarrier and symbol loop frequency and phase in formation to the 34-m antenna. However, when implementing FSC between a 70-m and 34-m antenna array, no aiding of the 34-m antenna is required since the carrier, subcarrier, and symbol timing loops operate on the combined signal as described in part 1 of this arti CIC. Furthermore, since it is difficul t for a single 34-m antenna to lock on to the signal by i tself, an array of four 34-m antennas is less effective using CSC than FSC. The differences mentioned above arc summarized in 'J'able 1.

As in the FSC case, the performance of CSC is measured both in terms of symbol SNR degradation and symbol SN1 ℓ loss. Symbol SNR degradation is defined as the ratio of the SNR at the matched filter output in the presence of non-ideal synchronization to the SNR in

the presence of ideal synchronization. On the other hand, symbol SNR loss is defined as the additional symbol SN1 R needed in the presence of imperfect synchronization to achieve the same symbol error rate (SER) as in the presence of perfect synchronization. Mathematical representations of degradation and loss for CSC are given in the next section. Afterwards, the performance of CSC and FSC are compared via various numerical examples. Some of the results derived in part 1 of this article are used to develop the degradation and loss theory for CSC. For the most part, the notations used here are self-contained but, in some instances, the reader is referred to part 1 of this article.

2 CSC Performance

As depicted in Fig. 1 (a), signals from multiple antennas in CSC are open-loop downconverted to baseband, partially demodulated using multiple subcarrier loops, multiple symbol loops, and multiple matched filters, then combined and demodulated using a single baseband carrier loop. The subcarrier and symbol loops used for CSC can be the same as those used in FSC, or they can be slightly modified versions which take advantage of both the I and Q components of the baseband signal. CSC implementations with the same loops as in the FSC would use either the I or Q component of the baseband signal. in either case, the loop SNR s of the subcarrier and symbol loops need to be re-computed as the loop input can no longer be assumed to have carrier lock. Let $\rho^{I}_{sc_n,csc}$ denote the loop SNR of the n^{th} subcarrier loop when either the I or Q arm is used (i.e., the unmodified loop), and let $\rho^{IQ}_{sc_n,csc}$ denote the subcarrier loop SNR when both the I and Q arms are used (i .e., the modified loop). Similarly define $\rho^{I}_{sy_n,csc}$ and $\rho^{IQ}_{sy_n,csc}$ for the n^{th} symbol loop. Then from Appendix A, it is shown that

$$\rho^{I}_{sc_n,csc} = \frac{2}{(\pi)} \frac{P_n/N_{0n}}{2W_{sc_n} B_{sc_n}} \left(1 + \frac{1}{P_n T/N_{0n}} \right)^{-1} \tag{1}$$

$$\rho^{I}_{sy_n,csc} = \frac{1}{2\pi^2} \frac{P_n/N_{0n}}{W_{sy_n} B_{sy_n}} \mathcal{L}_I \tag{2}$$

and

$$\rho_{sc_n,csc}^{IQ} = \left(\frac{2}{\pi}\right)^2 \frac{P_n/N_{0n}}{W_{sc_n}B_{sc_n}} \left(1 + \frac{1}{P_nT/N_{0n}}\right)^{-1} \quad (3)$$

$$\rho_{sy_n,csc}^{IQ} = \frac{1}{2\pi^2} \frac{P_n/N_{0n}}{W_{sy_n}B_{sy_n}} \mathcal{L}_{IQ} \quad (4)$$

where $W_{sc_n}B_{sc_n}$ and $W_{sy_n}B_{sy_n}$ are the window-loop bandwidth products of the n^{th} subcarrier and symbol loops, respectively; P_n and N_{0n}, denote respectively the signal power and one-sided noise power spectral density (1 'S1)) level of antenna n; and T is the symbol period in seconds. The squaring loss $\mathcal{L}_I$ for the unmodified loop and $\mathcal{L}_{IQ}$ for the modified loop are defined in Appendix A .2. For the Galileo scenario, it is shown that using the unmodified subcarrier and symbol loop reduces the loop SNR by 6 dB compared to the carrier locked case, and utilizing both the IQ-arm recovers 3 of the 6 dBs. Consequently, since the modified subcarrier and symbol loops result in an improved performance, they will be used in this article when comparing CSC to FSC.

Referring to Fig. 1 (a), the combining gain is maximized by aligning the baseband signals in time and phase, prior to combining. The alignment algorithm for an array of two antennas is shown in Fig. 1 (b). Here signal 1 is assumed to be delayed by m symbols with respect to signal 2. The signals are time aligned by delaying signal 2 by $\hat{m}$ symbols where $\hat{m}$ is an estimate of m. As in the FSC case, we assume perfect time alignment so that $\hat{m} = m$. After time alignment, the phase of signal 2 with respect to signal 1 is assumed to be θ_{21} radians. Hence, signal 2 is phase shifted by an amount equal to $-\hat{\theta}_{21}$, scaled by β_2 [2], and then combined with signal 1.

The analysis of CSC degradation and loss begins with the expression for the output of the matched filter in Fig. 1 (a). Note that there are actually $2L$ matched filters per L antennas because after subcarrier demodulation, a real symbol stream is modulated by I and Q baseband tones. Using complex notation, the matched filter output stream corresponding

to the k^{th} symbol and the n^{th} antenna, conditioned on ϕ_{sc_n} and ϕ_{sc_n}, can be written as

$$\tilde{v}_{k,n} = \begin{cases} \sqrt{P_n} C_{sc_n} d_k e^{j(\Delta\omega_c t_k + \theta_{n1})} + \tilde{n}_{k,n} & d_k = d_{k-1} \\ \sqrt{P_n} C_{sc_n} \left(1 - \frac{|\phi_{sy_n}|}{\pi}\right) d_k e^{j(\Delta\omega_c t_k + \theta_{n1})} + \tilde{n}_{k,n} & d_k \neq d_{k-1} \end{cases} \tag{5}$$

where the noise $\tilde{n}_{k,n}$ is a complex Gaussian random variable with variance No/7'. The subcarrier reduction function, C_{sc_n}, is given by[1] (6, part 1) after replacing ϕ_{sc} by ϕ_{sc_n}, the subcarrier phase error for loop n. 1 n addition, the phase ϕ_{sy_n} denotes the symbol synchronization phase error for loop n, and θ_{n1} is the phase relative to signal 1, i.e. θ_{11} = O. The baseband carrier frequency Δf_c or $\Delta\omega_c/2\pi$ is equal to the difference between the predicted and actual 1 F carrier frequency, and is assumed to be much less than the symbol rate, i .c., A f_c << 1 /7'. The degradation at the output of the matched filter when the carrier is open loop downconverted is approximately given as

$$D_{\Delta f_c} = \left(\frac{\sin(\pi \Delta f_c T)}{(\pi \Delta f_c T)}\right)^2 \tag{6}$$

Figure 2 illustrates the matched filter degradation as a function of $\Delta f_c T$, and it is clear that the degradation is less than 0.013 dB when $\Delta f_c T$ <0.03.

The combined signal after phase compensation, $\tilde{z}_k$ in Fig. 1 (a), is given as

$$\tilde{z}_k = \sum_{n=1}^{L} \beta_n \tilde{v}_{k,n} e^{-j\hat{\theta}_{n1}} \tag{7}$$

where $\tilde{v}_{k,n}$ is given in (5) and $\hat{\theta}_{n1}$ is an estimate of θ_{n1}. The optimum combiner weights arc given as [2]

$$\beta_n = \sqrt{\frac{P_n}{P_1} \frac{N_{01}}{N_{0n}}} \tag{8}$$

After substituting (5) for $\tilde{v}_{k,n}$ in ('7), the combined signal can be rewritten as follows (see Appendix B. 1)

$$\tilde{z}_k = \sqrt{P'} d_k e^{j(\Delta\omega_c t_k + \theta_{\tilde{z}})} + \tilde{n}_k \tag{9}$$

[1] The notation (6, partI) means equation 6 of part 1 of this article

where the variance of the combined complex noise is given as [2]

$$\sigma_{\tilde{n}}^2 = \frac{N_{01}}{T}\sum_{n=1}^{L}\gamma_n \tag{lo}$$

with $\gamma_n \triangleq \frac{P_1 N_{01}}{P_1 N_{0n}}$ 25[25, part I].e conditional combined signal power, P', is given as

$$P' = \begin{cases} P_1 \sum_{n=1}^{L}\sum_{m=1}^{L}\gamma_n\gamma_m C_{sc_n}C_{sc_m}C_{nm} & d_k = d_{k-1} \\ P_1 \sum_{n=1}^{L}\sum_{m=1}^{L}\gamma_n\gamma_m C_{sc_n}C_{sc_m}(1-\frac{|\phi_{sy_n}|}{\pi})(1-\frac{|\phi_{sy_m}|}{\pi})C_{nm} & d_k \neq d_{k-1} \end{cases} \tag{11}$$

where C_{nm} is presented in (27, part 1). 'J 'he signal $\tilde{z}_k$ is then demodulated using a baseband Costas loop with output equal to $e^{-j(\Delta\omega_c t_k + \hat{\theta}_{\tilde{z}})}$, where $\hat{\theta}_{\tilde{z}}$ is an estimate of $\theta_{\tilde{z}}$. The demodulator output is a real combined symbol stream and can be represented as

$$z_k = \sqrt{P'}C_c d_k + n_k \tag{12}$$

where C_c and P' are respectively given by (5, part]) and (1]). 'The noise n_k is a real Gaussian ran dom variable with variance $\sigma_n^2 = \frac{1}{2}\sigma_{\tilde{n}}^2$ where $\sigma_{\tilde{n}}^2$ is given by (1 O). The SNR conditioned on $\phi_c, \phi_{sc_n}, \phi_{sy_n}, \Delta\phi_{n1}$, denoted SNR'_{csc}, is defined as the square of the conditional mean of z_k divided by the conditional vari ance of z_k, i .e,

$$SNR'_{csc} = \begin{cases} \frac{2P_1T}{N_{01}}C_c^2\left(\frac{\sum_{n=1}^{L}\sum_{m=1}^{L}\gamma_n\gamma_m C_{sc_n}C_{sc_m}C_{nm}}{\sum_{n=1}^{L}\gamma_n}\right) & d_k = d_{k-1} \\ \frac{2P_1T}{N_{01}}C_c^2\left(\frac{\sum_{n=1}^{L}\sum_{m=1}^{L}\gamma_n\gamma_m C_{sc_n}C_{sc_m}(1-\frac{|\phi_{sy_n}|}{\pi})(1-\frac{|\phi_{sy_m}|}{\pi})C_{nm}}{\sum_{n=1}^{L}\gamma_n}\right) & d_k \neq d_{k-1} \end{cases} \tag{13}$$

'The last equation is useful in computing the symbol SNR degradation and loss for CSC as show]] below.

2.1 Degradation

'The degradation is found by dividing the unconditional CSC SNR which includes the effects of synchronization and alignment errors by the ideal SNR. 'J 'hc unconditional SNR, denoted SNR_{csc}, is computed by taking the statistical expectation of (13) with respect

to $\phi_c, \phi_{sc_n}, \phi_{sy_n}$, and $\Delta\phi_{n1}$. As in part I of this article, ϕ_c is assumed to be Tikhonov distributed, and ϕ_{sc_n} and ϕ_{sy_n} are assumed to be Gaussian distributed in addition, ϕ_{sc_m} and ϕ_{sc_n} are assumed **to** be independent when $n \neq m$, and the same is true for ϕ_{sy_m} and ϕ_{sy_n}. Consequently,

$$SNR_{csc} = \frac{2P_1T}{N_{01}}\overline{C_c^2}\,\frac{\left(\sum_{n=1}^{L}\gamma_n^2\overline{C_{sc_n}^2}\;\overline{C_{sy_n}^2} + \sum_{n=1}^{L}\sum_{\substack{m=1\\ n\neq m}}^{L}\gamma_n\gamma_m\overline{C_{sc_n}}\;\overline{C_{sc_m}}\;\overline{C_{sy_n}}\;\overline{C_{sy_m}}\;\overline{C_{nm}}\right)}{\sum_{n=1}^{L}\gamma_n} \tag{14}$$

where the average signal reduction function due to phase misalignment between baseband signals n and m, denoted C_{nm}, is given by (28, part I) with

$$\sigma^2_{\Delta\phi_{n1}} = \frac{1}{2SNR_{n1,csc}} \tag{15}$$

Here, $SNR_{n1,csc}$ denotes correlator SNR or [SNR of the complex signal $\tilde{x}$ in Fig. 1 (b)], and is shown in Appendix B.2 *to* equal

$$SNR_{n1,csc} = \frac{P_1}{N_{01}}\frac{T_c\overline{C_{sc_1}}^2\overline{C_{sc_n}}^2\overline{C_{sy_1}}^2\overline{C_{sy_n}}^2}{\overline{C_{sc_n}^2}\;\overline{C_{sy_n}^2} + \overline{C_{sc_1}^2}\;\overline{C_{sy_1}^2}\left(\frac{1}{\gamma_n}\right) + \frac{N_{0n}}{P_nT}} \tag{16}$$

where T_c is the averaging time of the correlator and T is the symbol period. The loop reduction functions $\overline{C_{sc_n}^2}$ an c1 $\overline{C_{sy_n}^2}$ for the nth subcarrier and symbol loops arc respectively given by (16, part I) and (17, part 1) where the loop SNRs in those equations are given by (3) and (4). Similarly, $\overline{C_{sc_n}}$ and $\overline{C_{sy_n}}$ can be computed using the same loop SNR as follows [3]

$$C_{sc_n} = 1 - \sqrt{\frac{8}{\pi^3}}\frac{1}{\sqrt{\rho_{sc_n}}} \tag{17}$$

$$C_{sy_n} = 1 - \frac{1}{2\pi^3}\frac{1}{\sqrt{\rho_{sy_n}}} \tag{18}$$

The carrier loop degradation $\overline{C_c^2}$ is given by (15, part 1) with the loop SNR ρ_c in that equation computed using the average combined power $P'/N_{0_{eff}}$ which is found by averaging (11) over all the phases and then dividing by the effective noise level, $N_{0_{eff}} = T\sigma_{\tilde{n}}^2$. I dean y when

there are no phase errors, $\overline{C_c^2} = \overline{C_{sc}^2} = \overline{C_{sy}^2} = \overline{C_{sc}} = \overline{C_{sy}} = \overline{C_{nm}} = 1$ and (14) reduces to $\left(\frac{2P_1T}{N_{01}}\sum_{n=1}^{L}\gamma_n\right)$ as expected. Dividing (14) by the ideal CSC SNR yields the degradation in dB, namely,

$$D_{csc} = -10\log_{10}\left(\overline{C_c^2}\left(\frac{\sum_{n=1}^{L}\gamma_n^2\overline{C_{sc_n}^2}\;\overline{C_{sy_n}^2} + \sum_{n=1}^{L}\sum_{\substack{m=1\\n\neq m}}^{L}\gamma_n\gamma_m\overline{C_{sc_n}}\;\overline{C_{sc_m}}\;\overline{C_{sy_n}}\;\overline{C_{sy_m}}\;\overline{C_{nm}}}{(\sum_{n=1}^{L}\gamma_n)^2}\right)\right) \tag{19}$$

2.2 Loss

The CSC SER for an L antenna array, denoted $P_{csc}(E)$, is defined as

$$P_{csc}(E) = \int_{-\frac{\pi}{2}}^{\frac{\pi}{2}}\oint_{-\infty}^{\infty}\oint_{-\infty}^{\infty}\oint_{-\infty}^{\infty} P'_{csc}(E)\,p_c(\phi_c)\prod_{i=1}^{L}\left[p_{\phi_{sc_i}}(\phi_{sc_i})p_{\phi_{sy_i}}(\phi_{sy_i})\right]\prod_{n=2}^{L}\left[p_{\Delta\phi_{n1}}(\Delta\phi_{n1})\right]\,d\boldsymbol{\Delta\phi}d\boldsymbol{\phi}_{sc}d\boldsymbol{\phi}_{sy}d\phi_c \tag{20}$$

where the three $\oint_{-\infty}^{\infty}$ are with respect to $\boldsymbol{\phi}_{sc} = (\phi_{sc_1}, \cdots, \phi_{sc_L})$, $\boldsymbol{\phi}_{sy} = (\phi_{sy_1}, \ldots, \phi_{sy_L})$, and $\boldsymbol{\Delta\phi} = (\Delta\phi_{21}, \ldots, \Delta\phi_{(L-1)1})$. Following similar steps as in the single antenna case of part 1, the conditional SER, denoted P'_{csc}, is given as

$$P'_{csc} = \frac{1}{4}\mathrm{erfc}\left[\sqrt{\frac{E_{s1}}{N_{01}}\frac{\left(\sum_{n=1}^{L}\gamma_n^2C_{sc_n}^2(1-\frac{|\phi_{sy_n}|}{\pi})^2 + \sum_{n=1}^{L}\sum_{\substack{m=1\\n\neq m}}^{L}\gamma_n\gamma_mC_{sc_n}C_{sc_m}(1-\frac{|\phi_{sy_n}|}{\pi})(1-\frac{|\phi_{sy_m}|}{\pi})C_{nm}\right)}{\sum_{n=1}^{L}\gamma_n}}C_c\right]$$
$$+\ \frac{1}{4}\mathrm{erfc}\left[\sqrt{\frac{E_{s1}}{N_{01}}\frac{(\sum_{n=1}^{L}\gamma_n^2C_{sc_n}^2 + \sum_{n=1}^{L}\sum_{\substack{m=1\\n\neq m}}^{L}\gamma_n\gamma_mC_{sc_n}C_{sc_m}C_{nm})}{\sum_{n=1}^{L}\gamma_n}}C_c\right] \tag{21}$$

where $E_{s1}/N_{01} = P_1T/N_{01}$ is the symbol SNR at antenna 1. Ideally, when there are no losses, $C_c = C_{sc_n} = \left(1-\frac{|\phi_{sy_n}|}{\pi}\right) = C_{nm} = 1$ and (20) reduces to $P(E)_{csc} = \frac{1}{2}\mathrm{erfc}(\sqrt{\frac{E_sL}{N_O}})$ for an array of L antennas of the same size (i.e., when $\gamma_n = 1$ for all n). The loss for CSC is given by (36, part 1) with $P_{fsc}(E)$ in that equation now replaced by (20).

3 Numerical Results and Discussion

The discussion section is divided into two parts. The first part describes CSC for an array of two 70-m antennas when the symbol SNR at each antenna is very low (-11 dB) and very high (6 dB). As in the case of FSC, results show that degradation and loss are equal at low SNR values, but that degradation is a lower bound for loss at high SNR values. The second part evaluates the performance of CSC and simultaneously compares it to the FSC performance described in part 1, The arraying gain for several different antenna combinations is computed using signal characteristics that are typical of the Galileo S-band mission to Jupiter.

3.1 Degradation vs. Loss

The CSC and FSC performance for an array of two 70-m antennas when the received signal is weak is shown in Fig. 3; results for a strong signal case are shown in Fig. 4(a) for B_c = 701 Hz, and Fig. **4(b)** for B_c = 160 Hz. inspection of these figures show that degradation and loss are equal (within 0.01 dB) for weak signal levels, but degradation is a lower bound for loss at strong signal levels. Consequently, degradation which in general is a relative performance measure can be used at low symbol SNRs to make an absolute assessment of the received system. Clearly, when all harmonics of the subcarrier are used (see section 3.2) FSC outperforms CSC except at narrow $W_{sc}B_{sc} = W_{sy}B_{sy}$ where both curves converge.

The weak and strong signals are the same as in the FSC example of Part 1. That is, weak signal: $\frac{P_1}{N_{01}} = \frac{P_2}{N_{02}} = 15$ dB-Hz, $R_{sym} = \frac{1}{T} = 400$ sym/sec, strong signal: $\frac{P_1}{N_{01}} = \frac{P_2}{N_{02}} = 32$ dB-Hz, $R_{sym} = \frac{1}{T} = 400$ sym/sec. For an ideal system with two equal antennas, the combined $\frac{E_s}{N_0}$ for the weak signal case is -8 dB which corresponds[2] to an SER = 0.286942, and the combined $\frac{E_s}{N_0}$ in the strong signal case is 9 dB for which the SER = 3.4 x 10-5. The receiver parameters for CSC and FSC in the weak signal case are assumed to be as follows:

[2] $P(E)_{ideal} = \frac{1}{2}\mathrm{erfc}\left(\sqrt{\frac{E_s}{N_o}L}\right)$ for L antennas of the same size.

B_c = 0.1 1 Iz, B_{sc} and B_{sy} are variable, B_{corr} = 4 kHz (applies for FSC only), and T_c = 120 seconds. The following parameters apply to the strong signal case: B_c = 7011 z and B_c = 160 Hz, B_{sc} and B_{sy} are variable, B_{corr} =- 4 k] Iz (applies for FSC only), and T_c = 120 seconds.

The degradation curves for CSC is found through (19), and the loss curves arc computed using (36, part 1) in conjunction with (20). The loss computation for CSC is an iterative process that uses the trial-and-error method described in part 1. The CSC subcarrier and symbol loop SN1 ts arc computed using (3) and (4) respectivel y. The carrier loop SNR for CSC is computed using the average combined power $P'/N_{0_{eff}}$, which is found by averaging (11) over all the phases and then dividing by the effective noise level. Morcover, the correlator SNRs for CSC were computed using (16).

3.2 Galileo S-band Mission Scenario

The CSC and FSC performance for different combinations of 70-m and 34-m antennas arc discussed in this section. Since the Galileo signal is a weak signal, the performance measure used is degradation, although loss could have also been used as demonstrated in Fig. 3. As pointed out in part I of this article, the 1 F signals in FSC arc typically transmitted to central location before being combined and demodulated using a single receiver. Duc to the finite bandwidth of the retransmission channel, 0.22 dB of 'the total energy is lost in FSC. The retransmission of CSC signals to a central location, on the other hand, dots not result in an energy loss because the symbol rates for Galileo (less than 640 sym/see) can be easil y supported by the retransmission channel.

3.2.1 Array of Two 70-m Antennas:

With that background, consider first an array of two 70-m antennas when the signal characteristi cs and receiver parameters arc the same as those in Fig. 3. The CSC degradation curve, which is the same as in Fig. 3 since no energy is lost in retransmission, is plotted in Fig. 5 along with the shifted FSC curves. Notice that both techniques have equal performance

when $W_{sc}B_{sc} = W_{sy}B_{sy} = 1.2$ mHz. In addition, Fig. 5 shows results using the same parameters as in Fig. 3 but now with $R_{sym} = 200$ sym/sec. in this case, CSC and FSC have equal performance when $W_{sc}B_{sc} = W_{sy}B_{sy} = 3.0$ mHz. The degradation due to individual components (carrier, subcarrier, symbol, and correlator) are discussed below to understand the relative contribution of each to the total degradation shown in Fig. 5 for $R_{sym} = 400$ Sym/sec.

The degradation due to a single component is defined as the degradation that would be observed when all but a single component is operating ideally. For example, in CSC the degradation due to the carrier loop is given as

$$D_{csc}\Big|_{\left[SNR_{n1,csc}=\rho^{IQ}_{sc_n,csc}=\rho^{IQ}_{sy_n,csc}=\infty\right]} = -10\log_{10}\overline{C_c^2} \tag{22}$$

which is derived by setting the correlator SNR, the subcarrier loop SNR, and the symbol loop SNR to infinity in (19). The degradation due to individual components is shown in Fig. 6(a), (b), (c), and (d). Table 4 lists the degradation break-down for CSC and FSC at $W_{sc}B_{sc} = W_{sy}B_{sy} = 5$ mHz. It is evident that the combiner degradation for both schemes is negligible. Also, the carrier degradation is the same for CSC and FSC since the carrier loop SNR for both schemes is about the same. The subcarrier and symbol degradation, however, are significantly different for CSC and FSC, the degradation from the former being greater than latter due to the carrier not being tracked and the signal not being combined until after the subcarrier and symbol loops. Comparing the sum in Table 4 to Fig. 3 for $R_{sym} = 400$ sym/sec indicates that the total degradation can be approximated to be the sum of the individual degradations.

3.2.2 Array of One 70-m and One 34-m STD Antennas:

The performance of a 70-m and one 34-m standard (STD) antenna array is shown in Fig. 7(a) using the same parameters as in Fig. 5 except $\frac{P_1}{N_{01}} = 15$ dB-Hz and $\frac{P_2}{N_{02}} = 7.3$ dB-Hz, i.e., $\gamma_1 = 1$ and $\gamma_2 = 0.17$ as shown in Table 1 of part 1. Figure 7(a) also shows the results

for *li.w,t=-* 200 sym/sec. At these signal levels the 34-m antenna is not expected to achieve subcarrier and symbol lock without being aided by the 70-m antenna. Consequently, the CSC arraying scheme is implemented by passing frequency and phase information from the 70-m to the 34-m antenna. As a result, the effective subcarrier and symbol loop SNRs of the 34-m is identical to that of the 70-m antenna. The modified CSC is called CSCA or Complex Symbol Combining with Aiding. in this scenario, the practical FSC outperforms CSCA when $W_{sc}B_{sc} = W_{sy}B_{sy}$ is greater than 4.5 mHz at R_{sym} = 400 sym/sec and 10.0 mHz at R_{sym} = 200 sym /sec.

3.2.3 Array of One **70-m** and Two **34-m STD** Antennas:

Result for an array of one 70-m and two 34-m antennas is shown in Fig. 7(b). Practical FSC, in this case, outperforms CSCA when $W_{sc}B_{sc} = W_{sy}B_{sy}$ is greater than 4.0 mHz at R_{sym} = ***400*** sym/sec and 8.5 mHz at R_{sym} = ***200*** sym/sec.

3.2.4 Array of One **70-m** and three **34-m STD** Antennas:

Result for an array of one 70-m and three 34-m antennas is shown in Fig. 7(c). Practical FSC outperforms CSCA when $W_{sc}B_{sc} = W_{sy}B_{sy}$ is greater than 3.5 mHz for R_{sym} = 400 sym/sec and 8.2 mHz for R_{sym} = 200 sym/sec.

3.2.5 Array of Four 34-m STD Antennas:

Result for an array of four 34-m antennas is shown in Fig. 7(d) for R_{sym} = 50 sym/sec and R_{sym} = 25 sym/sec with B_{corr} = 4001 Hz. For this array, FSC has less degradation than CSC when $W_{sc}B_{sc} = W_{sy}B_{sy}$ is above 0.32 mHz for R_{sym} = 50 sym/sec and 0.8 mHz for R_{sym} = 25 sym/sec. Practical FSC is able to operate for the given $W_{sc}B_{sc} = W_{sy}B_{sy}$ without losing lock (assume the subcarrier and symbol loops are able to lock to the input signal if their respective loop SNRs are greater than 12 dB). For CSC, however, the maximum $W_{sc}B_{sc} = W_{sy}B_{sy}$ that

can be supported without losing lock is about 0.9 m] Iz[3] at R_{sym}=50 sym/sec and 2 mIIz at R_{sym}=25 sym/sec. 'l'able 5 lists the break-mwn points for the different combination of a 70-m and 34-m antennas mentioned.

4 Conclusion

Part I and 11 of this article describes the performance of FSC and CSC in terms of symbol SNR degradation and symbol SNR loss. It is shown that both degradation and loss are approximate] y equal at low values of symbol SNI t but diverge at high SNI t values.

It is evident, that the relative performance of FSC and CSC depends critical] y on the scenario. Both systems perform wel 1 except when the subcarrier and symbol clocks are so unstable that a small $W_{sc}B_{sc} = W_{sy}B_{sy}$ can 't be used. For the following arrays - two 70-m antennas, onc 70-m and one 34-m antennas, one 70-m and two 34-m antennas, and one 70-m and three 34-m antennas - it is shown that FSC has less degradation than CSC when $W_{sc}B_{sc}$ = $W_{sy}B_{sy}$ is above 3.0, 10.0, 8.5, and 8.2 ml Iz at the symbol rate of 200 sym/see, and 1.2, 4 .5, 4.(), and 3.5 mIIz at a symbol rate of 40() synl/see, respectively. For an array of four 34-m antennas, FSC has less degradation than CSC when $W_{sc}B_{sc}$ - $W_{sy}B_{sy}$ is above 0.32 ml Iz at the symbol rate of 50 sym/sec and above 0.8 ml 1 z at the symbol rate of 25 sym/sec.

[3]This point, however, can be increased by using the average of the four phase estimates of the subcarrier and symbol loops to effectivel y improve the loop SNR by about 6 dB, so that the degradation is lessened.

Appendix A

A.1 Subcarrier Loop SNR Performance

Compared to the conventional unmodified subcarrier loop which employs the I-arm as shown in Fig. A. 1, the modified subcarrier loop, depicted in Fig. A.2, utilizes both the I and Q arms of the baseband signal for tracking. The loop SNR for both schemes are derived here and compared to the case when the carrier is locked. For CSC, the I and Q channels at the input of the subcarrier loop are respectively given as

$$I(t_n) = \sqrt{P}d(t_n)\mathrm{Sqr}(\omega_{sc}t_n + \theta_{sc})\cos(\Delta\omega_c t_n) + n_I(t_n) \tag{A.1}$$

$$Q(t_n) = \sqrt{P}d(t_n)\mathrm{Sqr}(\omega_{sc}t_n + \theta_{sc})\sin(\Delta\omega_c t_n) + n_Q(t_n) \tag{A.2}$$

where $n_I(t_n)$ and $n_Q(t_n)$ are independent Gaussian noise processes and all other parameters are previously defined. As shown in Fig. A.2, both the I and Q components are multiplied by the squarewave references and averaged over one symbol period (assuming perfect symbol timing), resulting in [4]

$$I_s(k) = \sqrt{P}d_k f(\phi_{sc})\cos(\Delta\omega_c t_k) + n_{Is}(k) \tag{A.3}$$

$$I_c(k) = \sqrt{P}d_k g(\phi_{sc})\cos(\Delta\omega_c t_k) + n_{Ic}(k) \tag{A.4}$$

$$Q_s(k) = \sqrt{P}d_k f(\phi_{sc})\sin(\Delta\omega_c t_k) + n_{Qs}(k) \tag{A.5}$$

$$Q_c(k) = \sqrt{P}d_k g(\phi_{sc})\sin(\Delta\omega_c t_k) + n_{Qc}(k) \tag{A.6}$$

where k denotes the symbol index, $f(\phi_{sc}) = 1 - \frac{2}{\pi}|\phi_{sc}|$ for $|\phi_{sc}| \le \pi$, $g(\phi_{sc}) = \frac{2}{\pi}\phi_{sc}$ for $|\phi_{sc}| \le \frac{\pi W_{sc}}{2}$, and $\mathrm{Var}[n_{Is}(k)] = \mathrm{Var}[n_{Ic}(k)] = \mathrm{Var}[n_{Qs}(k)] = \mathrm{Var}[n_{Qc}(k)] = \sigma_n^2 = \frac{N_0}{2T}$. The error signal of the conventional and modified subcarrier loops are respectively given as

$$e(k)_I = Pf(\phi_{sc})g(\phi_{sc})\cos^2(\Delta\omega_c t_k) + N_I(k) \tag{A.7}$$

$$e(k)_{IQ} = Pf(\phi_{sc})g(\phi_{sc}) + N_{IQ}(k) \tag{A.8}$$

where the variance of the noise terms (after averaging over $\Delta\omega_c t_k$ assuming uniform distribution) are respectively given as

$$\sigma^2_{N_{IQ}} = P\sigma_n^2 + 2\sigma_n^4 \tag{A.9}$$

$$\sigma^2_{N_I} = \frac{P\sigma_n^2}{2} + \sigma_n^4 \tag{A.10}$$

The slope of the S-curve can now be found by taking the first derivative of the average error signal with respect to ϕ_{sc}, and then setting $\phi_{sc} = 0$. Accordingly, the slopes of the conventional and modified subcarrier loop are given as

$$K^I_{g,sc} = \frac{1}{\pi} \tag{A.11}$$

$$K^{IQ}_{g,sc} = \frac{2}{\pi} P \tag{A.12}$$

Note the slope of the IQ-arm is identical to the slope of the I-arm when the carrier is locked [4]. Assuming linear theory, the loop SNR for the subcarrier loop is given as

$$\rho_{sc} = \frac{1}{2B_{sc}T} \frac{K_g^2}{} \tag{A.13}$$

where B_L is the One-sided noise bandwidth of the loop. Simplifying, the conventional and modified loop SNRs are respectively given as

$$\rho^I_{sc} = \left(\frac{2}{\pi}\right)^2 \frac{P/N_0}{2B_L W_{sc}} \left(1 + \frac{1}{PT/N_0}\right)^{-1} \tag{A.14}$$

$$\rho^{IQ}_{sc} = \left(\frac{2}{\pi}\right)^2 \frac{P/N_0}{B_{sc} W_{sc}} \left(1 + \frac{1}{PT/N_0}\right)^{-1} \tag{A.15}$$

For comparison, the I-arm loop SNR when the carrier is locked is given in (10, part 1). Figure A.3 illustrates the subcarrier loop SNRs when the I-arm, IQ-arm, and the I-arm with the carrier locked are used. For low symbol SNRs, the I-arm has a loop SNR that is 6 dB lower than the case when the carrier is locked. Using the IQ-arm, however, recovers 3 of the 6 dBs. At high symbol SNRs, the performance of the IQ-arm is identical to the I-arm when the carrier is locked.

A.2 Digital Data Transition Tracking Loop SNR Performance

Similar to the subcarrier loop, the conventional 1)igital 1)ata Transition TrackingLoop (1)'1''1'1,) shown in Fig. A.4 will be modified to utilize both the I and Q channels as depicted in Fig. A.5. Assuming perfect subcarrier demodulation, the 1 and Q components for CSC are given as

$$I_k = \sqrt{P} d_k \cos\phi_c + n_k^I \tag{A.16}$$

$$Q_k = \sqrt{P} d_k \sin\phi_c + n_k^Q \tag{A.17}$$

where n_k^I and n_k^Q arc independent Gaussian random variables with variance $\sigma_n^2 = \frac{N_0}{2T}$ and ϕ_c is the carrier predi ct error,

The performance of the DTTL has been derived in [5] assuming carrier lock ($\phi_c = 0$). When this is not the case as in CSC, the loop suffers degradation and the objective here is to quantify the decrease in performance for both the conventional and modified 1)'] 'TL. The analysis of the 1)"1''1'1, follows closel y that of [5] with the difference now being that the data is modulated by a slow] y varying cosi ne function. Hence, all the relevant parameters arc derived here conditioned on ϕ_c and, afterwards, these parameters arc averaged over ϕ_c assuming uniforml y di stributed from --7r to π.

The normalized mean of the error signal, e_k, conditioned on the normalized timing error λ (in cycles) and the carrier predict error ϕ_c is the normalized phase detector characteristic $g_n(\lambda, \phi_c)$ commonl y termed the loop S-curve. Following similar steps as in [5], $g_n^I(\lambda, \phi_c)$ and $g_n^{IQ}(\lambda, \phi_c)$, the S-curves of the conventional and the modified 1)TTL, arc respectivel y given as

$$g_n^I(\lambda, \phi_c) = \lambda|\cos\phi_c|\mathrm{erf}(B) - \frac{W_{sy} - 2\lambda}{8}|\cos\phi_c|\,[\mathrm{erf}(A) - \mathrm{erf}(B)] \tag{A.18}$$

$$g_n^{IQ}(\lambda, \phi_c) = \lambda|\cos\phi_c|\mathrm{erf}(B) + \lambda|\sin\phi_c|\mathrm{erf}(B') - \frac{W_{sy} - 2\lambda}{8}|\cos\phi_c|\,[\mathrm{erf}(A) - \mathrm{erf}(B)] - \frac{w - 2\lambda}{8}|\sin\phi_c|\,[\mathrm{erf}(A') - \mathrm{erf}(B')] \tag{A.19}$$

where $A = \sqrt{\frac{E_s}{N_0}}|\cos\phi_c|$, $A' = \sqrt{\frac{E_s}{N_0}}|\sin\phi_c|$, $B = \sqrt{\frac{E_s}{N_0}}(1 - 2\lambda)|\cos\phi_c|$, and $B' = \sqrt{\frac{E_s}{N_0}}(1 - 2\lambda)|\sin\phi_c|$. To compute the S-curve conditioned only on λ, $g_n^I(\lambda, \phi_c)$ and $g_n^{IQ}(\lambda, \phi_c)$ are numerically integrated over ϕ_c assuming uniformly distributed. Setting $\phi_c = 0$ in (A, 18) results in the same S-curve as in [5]. The first derivative of the S-curve at $\lambda = 0$ is given as

$$K_{g,sy}^I(\phi_c) = |\cos\phi_c|\mathrm{erf}(A) - \frac{W_{sy}}{2}\cos^2\phi_c\sqrt{\frac{E_s}{N_0\pi}}\exp(-A^2) \tag{A.20}$$

$$\begin{aligned} K_{g,sy}^{IQ}(\phi_c) = {} & |\cos\phi_c|\mathrm{erf}(A) - \frac{W_{sy}}{2}\cos^2\phi_c\sqrt{\frac{E_s}{N_0\pi}}\exp(-A^2) \\ & + |\sin\phi_c|\mathrm{erf}(A') - \frac{W_{sy}}{2}\sin^2\phi_c\sqrt{\frac{E_s}{N_0\pi}}\exp(-A'^2) \end{aligned} \tag{A.21}$$

where $K_{g,sy}^I(\phi_c)$ and $K_{g,sy}^{IQ}(\phi_c)$ denote the slope of the S-curve for the conventional and modified DTTL conditioned on ϕ_c respectively. Numerically integrating over ϕ_c gives the unconditional slopes denoted as $K_{g,sy}^I$ and $K_{g,sy}^{IQ}$ respectively. Setting $\phi_c = 0$ in (A .20) gives

$$K_{g,sy} = \mathrm{erf}\left(\sqrt{\frac{E_s}{N_0}}\right) - \frac{W_{sy}}{2}\sqrt{\frac{E_s}{N_0\pi}}\exp\left(-\frac{E_s}{N_0}\right) \tag{A.22}$$

which is identical to the slope given in [5]. Figure A.6 lists the ratio of $\frac{K_{g,sy}^I}{K_{g,sy}}$ and $\frac{K_{g,sy}^{IQ}}{K_{g,sy}}$ for different symbol SNRs. At low symbol SNR, $K_{g,sy}$ and $K_{g,sy}^{IQ}$ are about the same while $K_{g,sy}^I$ is about, twice as large. Also, the normalized noise spectrum at $\lambda = 0$ can be shown to be

$$h^I(0, \phi_c) = 1 + 0.5W_{sy}\frac{E_s}{N_0}\cos^2\phi_c - \frac{W_{sy}}{2}\left[\frac{1}{\sqrt{\pi}}\exp(-A^2) + \sqrt{\frac{E_s}{N_0}}|\cos\phi_c|\mathrm{erf}(A)\right]^2 \tag{A.23}$$

$$\begin{aligned} h^{IQ}(0, \phi_c) = {} & 1 + 0.5W_{sy}\frac{E_s}{N_0} - \frac{W_{sy}}{2}\left[\frac{1}{\sqrt{\pi}}\exp(-A^2) + \sqrt{\frac{E_s}{N_0}}|\cos\phi_c|\mathrm{erf}(A)\right]^2 \\ & - \frac{W_{sy}}{2}\left[\frac{1}{\sqrt{\pi}}\exp(-A'^2) + \sqrt{\frac{E_s}{N_0}}|\sin\phi_c|\mathrm{erf}(A')\right]^2 \end{aligned} \tag{A.24}$$

where $h^I(0, \phi_c)$ and $h^{IQ}(0, \phi_c)$ denote the normalized noise spectrum for the conventional and modified DTTL conditioned on ϕ_c, respectively. Numerically integrating over ϕ_c results

in the unconditional normalized noise spectrum denoted as $h^I(0)$ and $h^{IQ}(0)$ respectivel y. Setting ϕ_c =- O in (A.23) gives

$$h(0) = 1 + 0.5W_{sy}\frac{E_s}{N_0} - \frac{W_{sy}}{2}\left[\frac{1}{\sqrt{\pi}}\exp\left(-\frac{E_s}{N_0}\right) + \sqrt{R_s}\,\mathrm{erf}\left(\sqrt{\frac{E_s}{N_0}}\right)\right]^2 \tag{A.25}$$

which is the same as the noise spectrum given in [5]. Figure A.7 lists values of h(0), h'(0), and $h^{IQ}(0)$ for different symbol SNRs. It is evident that $h(0)$ is slightly greater than $h^I(0)$ but significantly less than $h^{IQ}(0)$. Assuming linear theory, the DTTL loop SNR is given as [5]

$$\rho_{sy} = \frac{1}{2\pi^2}\frac{P}{N_0 W_{sy} B_{sy}}\mathcal{L} \tag{A.26}$$

where $\mathcal{L} = \frac{(K_{g_1 sy}\epsilon^2}{h(0)}$. Furthermore, the loop SNR for the conventional and modified DTTL, denoted ρ^I_{sy} and ρ^{IQ}_{sy}, are found by normalizing (A .26) by $\mathcal{L}^I = \frac{(K^I_{g_1 sy})^2}{h^I(0)}$ or $\mathcal{L}^{IQ} = \frac{(K^{IQ}_{g_1 sy})^2}{h^{IQ}(0)}$ respectively. Figure A.8 illustrates the loop SNR of the DTTL using the I-arm, IQ-arm, and I-arm when the carrier is locked, At low symbol SNI t, it is clear that, using on] y the I-arm reduces the loop SNR by 6 dB compared to the case when the carrier is locked, and utilizing the IQ-arm recovers 3 of the 6 dBs.

Appendix B

B.1 Derivation of (9)

Substituting (5) into (7) yields

$$\tilde{z}_k = \begin{cases} \sum_{n=1}^{L} \beta_n \sqrt{P_n} C_{sc_n} d_k e^{[j(\Delta\omega_c t_k + \Delta\phi_{n1})]} + \tilde{n}_{k,n} e^{[-j(\hat{\theta}_{n1})]} & d_k = d_{k-1} \\ \sum_{n=1}^{L} \beta_n \sqrt{P_n} C_{sc_n} (1 - \frac{|\phi_{sy_n}|}{\pi}) d_k e^{[j(\Delta\omega_c t_k + \Delta\phi_{n1})]} + \tilde{n}_{k,n} e^{[-j(\hat{\theta}_{n1})]} & d_k \neq d_{k-1} \end{cases} \tag{B.1}$$

where $\Delta\phi_{n1} = \theta_{n1}$ –&l and all other symbols are defined in (5) of main text. The conditional combined power, denoted P', in (9) is found by deriving the conditional mean of $\tilde{z}_k$; i.e.

$$P' = E(\tilde{z}_k/\phi_{sc_n}, \phi_{sy_n}, \Delta\phi_{n1}) E^*(\tilde{z}_k/\phi_{sc_m}, \phi_{sy_m}, \Delta\phi_{m1})$$

$$= \begin{cases} \sum_{n=1}^{L} \beta_n \beta_m \sqrt{P_n}\sqrt{P_m} C_{sc_n} C_{sc_m} e^{j[\Delta\phi_{n1} - \Delta\phi_{m1}]} & d_k = d_{k-1} \\ \sum_{n=1}^{L}\sum_{m=1}^{L} \beta_n \beta_m \sqrt{P_n}\sqrt{P_m} C_{sc_n} C_{sc_m} (1 - \frac{|\phi_{sy_n}|}{\pi})(1 - \frac{|\phi_{sy_m}|}{\pi}) e^{j[\Delta\phi_{n1} - \Delta\phi_{m1}]} & d_k \neq d_{k-1} \end{cases} \tag{B.2}$$

which simplifies to (11). In addition, the phase $\theta_{\tilde{z}}$ in (9) is given as

$$\theta_{\tilde{z}} = \begin{cases} \tan^{-1}\dfrac{\left(\sum_{n=1}^{L}\beta_n\sqrt{P_n}C_{sc_n}\cos(\Delta\omega_c t_k + \Delta\phi_{n1})\right)}{\left(\sum_{n=1}^{L}\beta_n\sqrt{P_n}C_{sc_n}\sin(\Delta\omega_c t_k + \Delta\phi_{n1})\right)} & d_k = d_{k-1} \\ \tan^{-1}\dfrac{\left(\sum_{n=1}^{L}\beta_n\sqrt{P_n}C_{sc_n}\left(1-\frac{|\phi_{sy_n}|}{\pi}\right)\cos(\Delta\omega_c t_k + \Delta\phi_{n1})\right)}{\left(\sum_{n=1}^{L}\beta_n\sqrt{P_n}C_{sc_n}\left(1-\frac{|\phi_{sy_n}|}{\pi}\right)\sin(\Delta\omega_c t_k + \Delta\phi_{n1})\right)} & d_k \neq d_{k-1} \end{cases} \tag{B.3}$$

B.2 Derivation of (16)

Let C_{sy_n} be the signal reduction function due to symbol timing errors in the n^{th} symbol synchronization loop. Then the n^{th} matched filter output in (5) can be rewritten as

$$\tilde{v}_{k,n} = \sqrt{P_n}C_{sc_n}\, C_{sy_n} d_k e^{[j(\Delta\omega_c t_k + \theta_{n1})]} + \tilde{n}_{k,n} \tag{B.4}$$

where

$$C_{sy_n} = \begin{cases} 1 & d_k = d_{k-1} \\ \left(1 - \frac{|\phi_{sy_n}|}{\pi}\right) & d_k \neq d_{k-1} \end{cases} \tag{B.5}$$

The relative phase difference between antenna n and 1 is estimated by performing the correlation operation shown in Fig. 2(L). Assuming perfect time alignment, the correlator output, $\tilde{x}$, is given as

$$\tilde{x} = \sum_{k=1}^{N} \tilde{v}_{k,n}\tilde{v}^*_{k,1} \tag{B.6}$$

where $N = T_c/T$ is the number of symbols used in the correlation. Substituting the expressions for $\tilde{v}_{k,n}$ and $\tilde{v}^*_{k,1}$ into (B.6) yields

$$\tilde{x} = \sqrt{P_1 P_n}C_{sc_1}C_{sc_n}C_{sy_1}C_{sy_n}e^{j(\theta_{n1})} + n_{\tilde{x}} \tag{B.7}$$

where

$$\mathrm{Var}(n_{\tilde{x}}) = 2P_1\overline{C^2_{sc_1}}\;\overline{C^2_{sy_1}}\;\frac{N_{0n}}{2T_c} + 2P_n\overline{C^2_{sc_n}}\;\overline{C^2_{sy_n}}\;\frac{N_{01}}{2T_c} + 2\frac{N_{01}N_{0n}}{2TT_c} \tag{B.8}$$

Using (A .5, part J), the correlator SNR between antenna n and 1 for CSC is given as

$$SNR_{n1,csc} = \frac{\sqrt{P_1P_n}\;\overline{C_{sc_1}}\;\overline{C_{sc_n}}\;\overline{C_{sy_1}}\;\overline{C_{sy_n}}}{2P_1\overline{C^2_{sc_1}}\;\overline{C^2_{sy_1}}\;\frac{N_{0n}}{2T_c} + 2P_n\overline{C^2_{sc_n}}\;\overline{C^2_{sy_n}}\;\frac{N_{01}}{2T_c} + 2\frac{N_{01}N_{0n}}{2TT_c}} \tag{B.9}$$

and simplifying yields (16).

Acknowledgments

The authors would like to thank Dr. William J. 1 Iurd for suggesting CSC as an arraying scheme. We wish to also thank Dr. Van Snider and Dr. Fred Vance for their numerical integration comments. Also, the various discussions with Joseph Statman, Pravin Vazirani, Dr. Steve Towncs, Jeff Berner, Alexander Milcant, Mazen Shihabi, Mimi Aung-Goodman, and Scott Stephens are greatly acknowledged.

References

1. S. Hinedi, "NASA's Next Generation All-Digital Deep Space Network Breadboard Receiver," *IEEE Trans. on Commun.*, vol. 41, pp. 246-257, January 1993.

2. D. Divsalar, "Symbol Stream Combining Versus Baseband Combining for Telemetry Arraying," *TDA Progress Report* 12-74, vol. April-June 1983, Jet 1'repulsion Laboratory, Pasadena, California, pp. 13-28, August 15, 1983.

3. A. Milcant and S. Hinedi, "Overview of Arraying Techniques for Deep Space Communications," to be pub] ished in *IEEE Trans. Commun.*

4. W. J. Hurd and S. Aguirre, "A Method to 1)ramatically 1 mprove Subcarrier Tracking," *IEEE Trans. on Commun.*, *vol.* 36, pp. 238-243, February 1988.

5 M. 1<, Simon, "Analysis of the Steady State 1 'hase Noise 1'erformance of a Digital Data-Transition Tracking Loop", Jet]'repulsion 1,aboratory, Pasadena, California, Space Programs Summary 37-55, vol. 3, pp. 54-62, February, 1969.

6. W. C. Lindsey and M. K. Simon, *Telecommunication Systems Engineering*, New Jersey: Prentice-Hall,]nc., 1973.

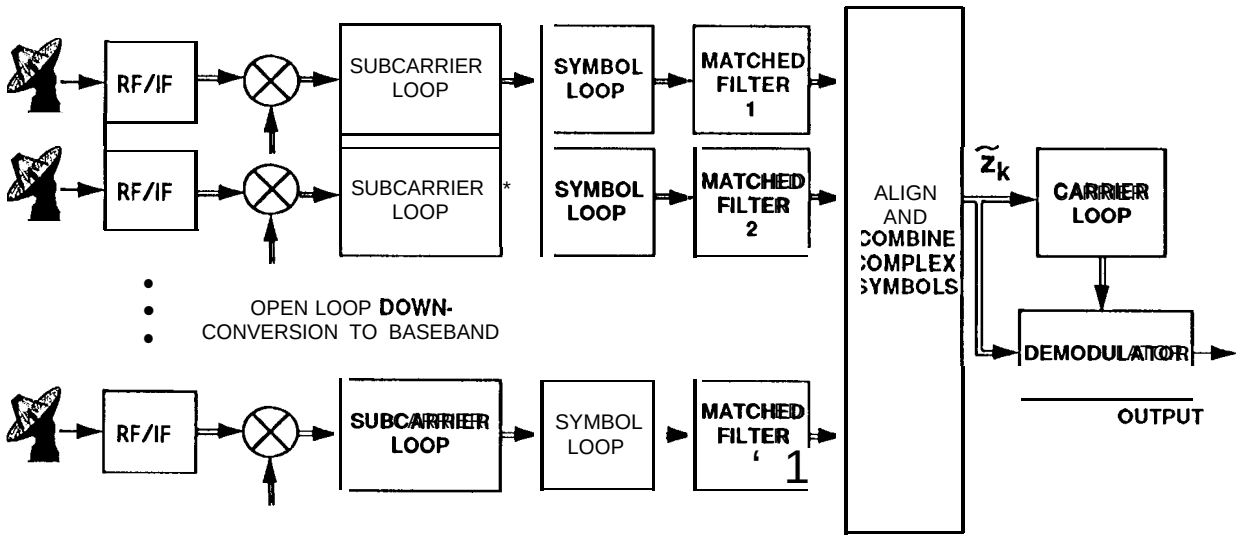

Figure la, Complex Symbol Combining (CSC)

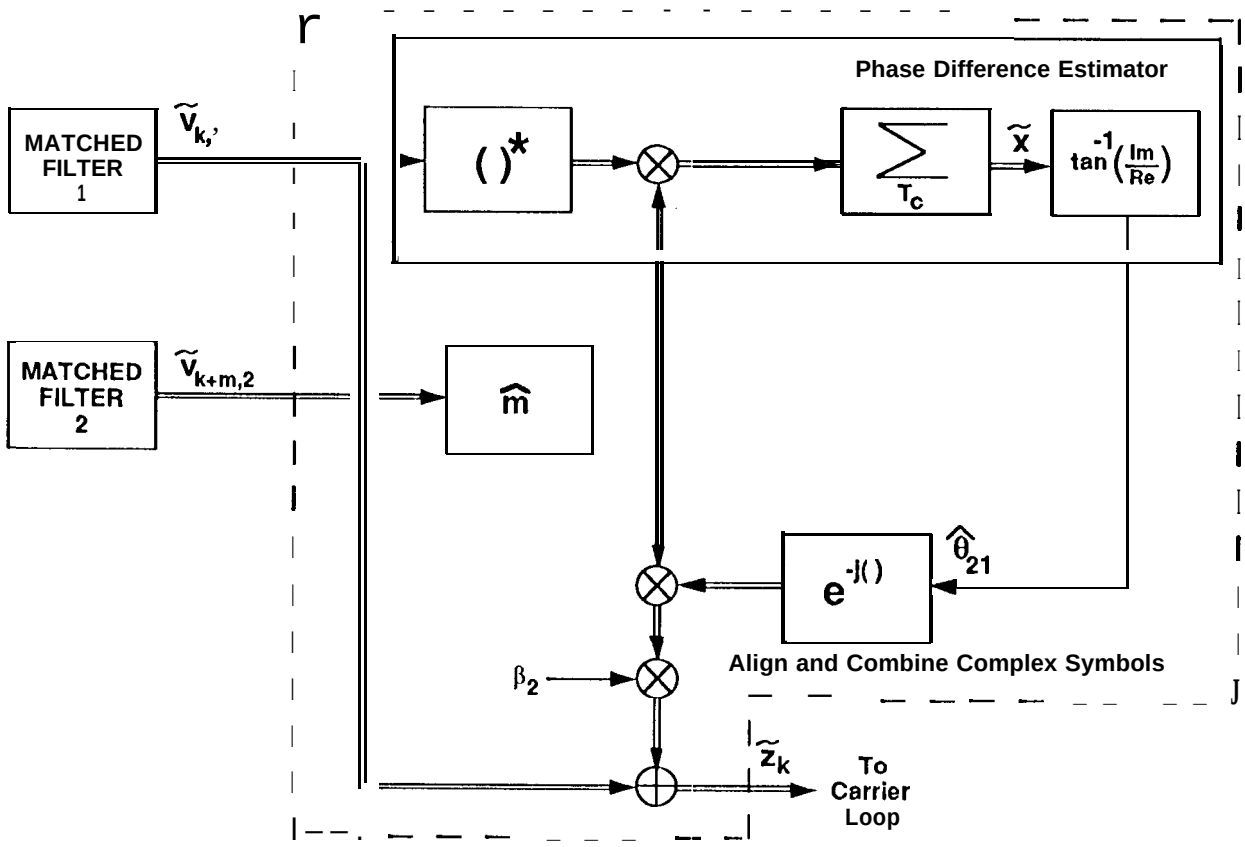

Figure 1 b. CSC Align and Combine algorithm for an array of two antennas

Table 1. Comparison of FSC and CSC

	FSC	Csc
Combining Bandwidth	Sample rate	Symbol rate
Carrier Loop	Closed before subcarrier and symbol loops	Closed after subcarrier and symbol loops
Effective P/No at input of SubCarrier loop for two 70-m antennas		At Least 6 dB Lower than FSC when the carrier is not locked and 3 dB lower than when the carrier is locked
Effective P/No at input of Symbol loop for two 70-m antennas		At Least 6 dB Lower than FSC when the carrier is not locked and 3 dB lower than when the carrier is locked
Array of a 70- and 34 m antenna	Loops operate on the combined signal power	Phase and frequency information passed from 70- to 34-meter antenna
Array of four 34-m antennas	Implementable	Harder to implement

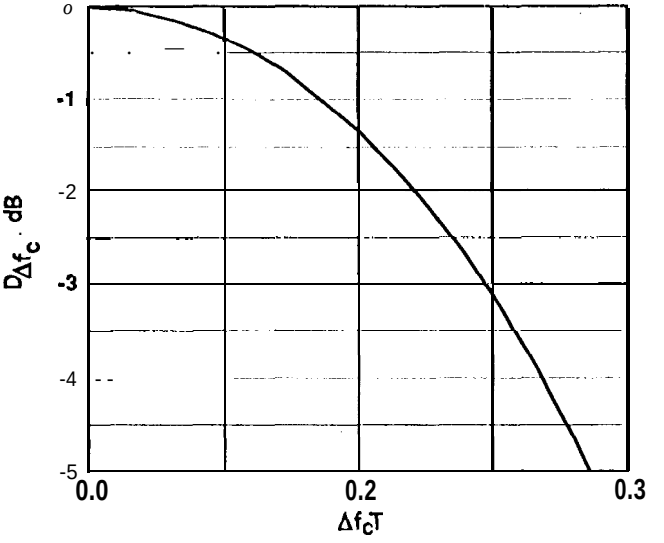

Figure 2. Degradation at the matched filter output vs. carrier frequency error-symbol time product

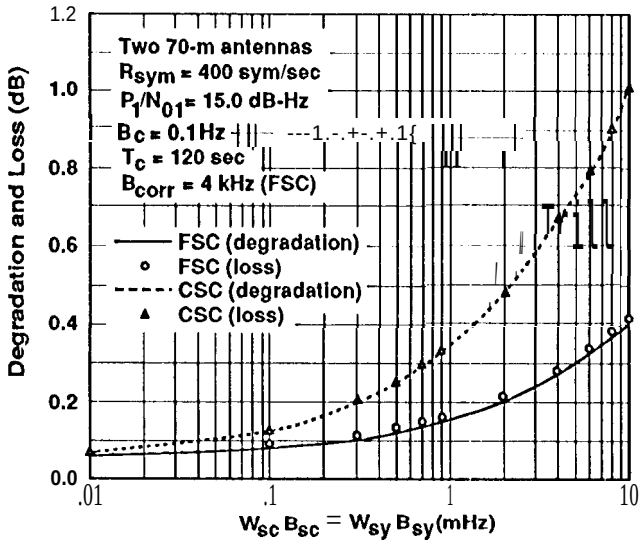

Figure 3. Degradation andloss vssubcarrier and symbol window-loop bandwidth for SER = 0.286942

Table 2. CSC loop SNRS for SER = 0.286942

$W_{sc}B_{sc} = W_{sy}B_{sy}$ (mHz)	Carrier Loop SNR (dB)	Subcarrier Loop SNR (dB)	Symbol Loop SNR (dB)	Correlator SNR (dB)
0.01	21.8	49.7	37.2	24.1
0,1	21.6	39,7	27.2	24.0
0.3	21.5	35.0	22.5	23.8
0.5	21.4	32,7	20.2	23.7
0.7	21.4	31.3	18.8	23.7
0,9	21.3	30.2	17.7	23.6
2,0	21.1	26.7	14.2	23.3
4,0	20.8	23.7	11.2	23.0
6.0	20.5	21.9	9.4	22.7
8.0	20.3	20.7	8 . 2	22.5
10,0	20.1	19.7	7.2	22.3

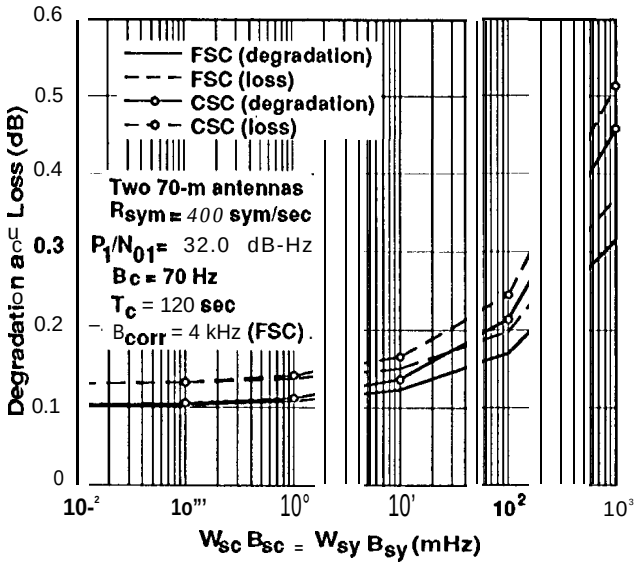

Figure 4a. Degradation and loss vs subcarrier and symbol window-loop bandwidth for SER = 3.4e-5 and B_C = 70 Hz

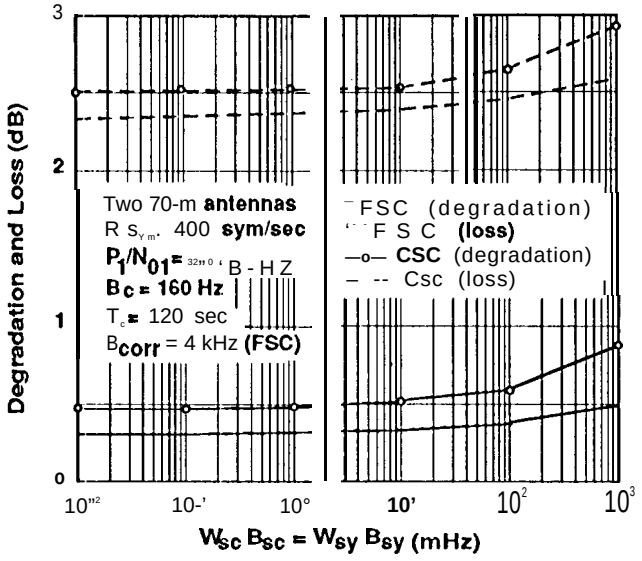

Figure 4b. Degradation and loss vs subcarrier and symbol window-loop bandwidth for SER = 3.4e-5 and B_C = 160 Hz

Table 3. CSC loop SNRS for SER = 3.4e-5

$W_{sc}B_{sc} = W_{sy}B_{sy}$ (mHz)	Carrier Loop SNR (dB)		Subcarrier Loop SNR (dB)	Symbol Loop SNR (dB)	Correlator SNR (dB)
	B_C = 160 Hz	B_C = 70 Hz			
0.01	12,7	16.3	77.1	67.3	49.3
0.1	12.7	16.3	67.1	57.3	49.3
1.0	12,7	16.3	57.1	47.3	49.3
10.0	12.7	16.3	47.1	37.3	49,2
100.0	12.6	16.2	37.1	27.3	49,1
1000,0	12.3	15.9	27.1	17.3	48.7

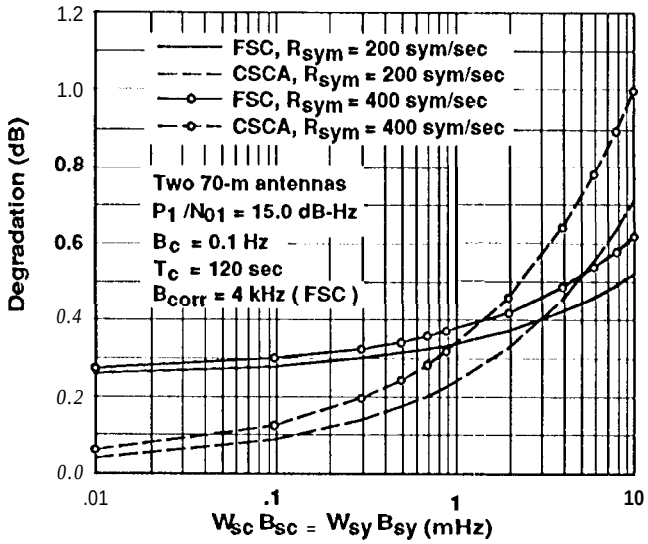

Figure 5. Practical FSC and CSC degradation vs subcarrier and symbol window-loop bandwidth

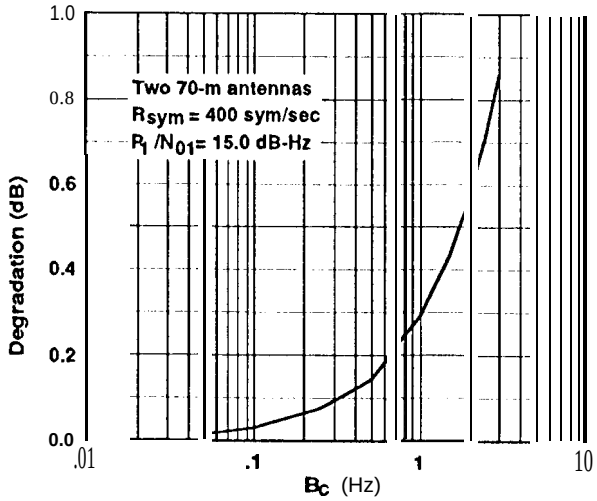

Figure 6a: Carrier Degradation vs Carrier Bandwidth

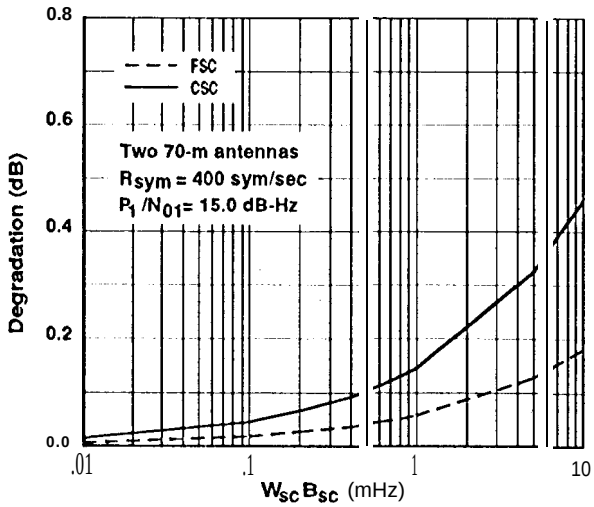

Figure 6b: Subcarrier Degradation vs Subcarrier window-loop Bandwidth

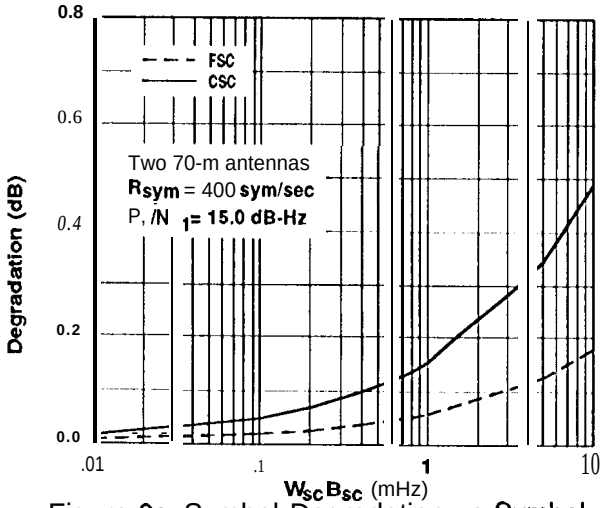

Figure 6c: Symbol Degradation vs Symbol window-loop-Bandwidth

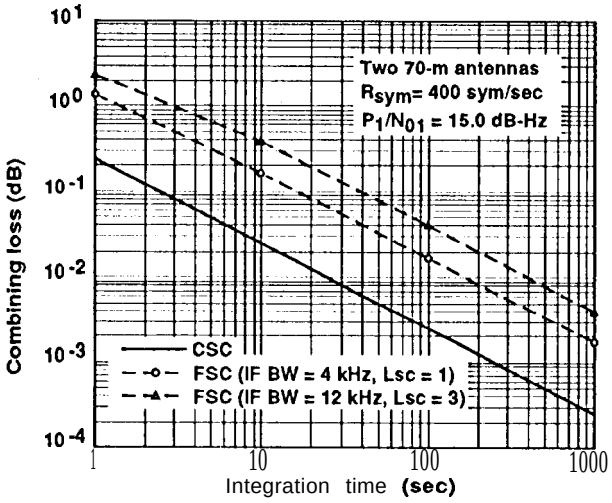

Figure 6d: Combining Loss vs Integration Time

Degradation	FSC	CSC
Combiner	0.034 dB	0.002 dB
Carrier Loop	0.029 dB (ρ_c =21.8 dB)	0.038 dB (ρ_c = 20.6 dB)
Subcarrier Loop	0.126 dB (ρ_{sc} = 30.8 dB)	0.324 dB (ρ_{sc} = 22.7 dB)
Symbol Loop	0.124 dB (ρ_{sy} = 19.0 dB)	0.342 dB (ρ_{sy} = 10.2 dB)
Energy Loss	0.22 dB	0 dB
Sum	0.533 dB	0.708 dB

Table 4. Degradation Breakdown for two 70-m antennas at W_{SC} Bs_c = W_{sy} B_{sy} = 5mHz

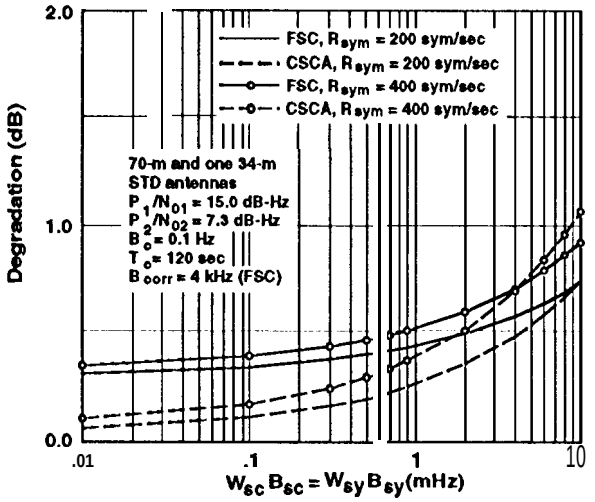

Figure 7a. Degradation for an array of one 70-m and one 34-m STD antennas

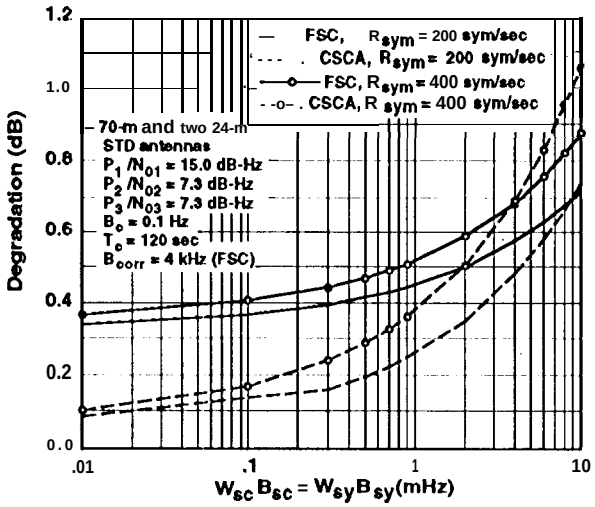

Figure 7b. Degradation for an array of one 70-m and two 34-m STD antennas

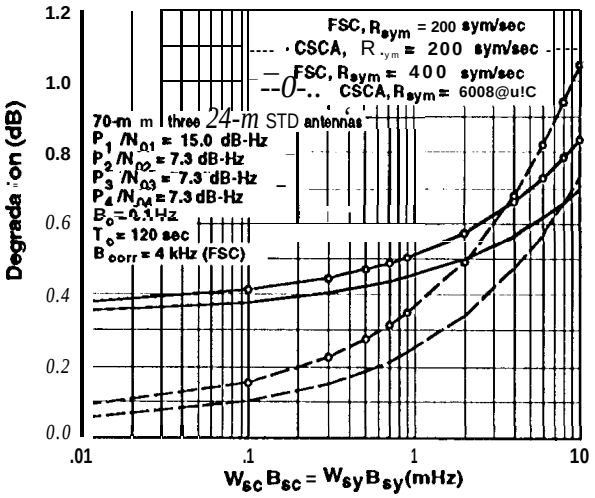

Figure 7c. Degradation for an array of one 70-m and three 34-m STD antennas

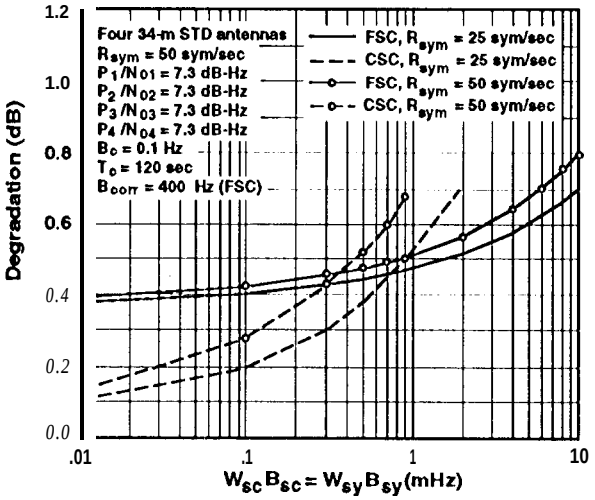

Figure 7d. Degradation for an array of four 34-m STD antennas

Table 5. Break-even point for FSC and CSC

Antenna Array	Value of $W_{sy}B_{sy} = W_{sc}B_{sc}$ (mHz) where $D_{fsc} = D_{csc}$		Value of $W_{sy}B_{sy} \cdot W_{sc}B_{sc}$ (mHz) where $D_{fsc} > D_{csc}$		Value of $W_{sy}B_{sy} = W_{sc}B_{sc}$ (mHz) where $D_{fsc} < D_{csc}$	
	R_{sym} = 200 Hz	R_{sym} = 400 Hz	ym = 200 Hz	R_{sym} = 400 Hz	R_{sym} = 200 Hz	R_{sym} = 400 Hz
Two 70-m	3.0	1.2	>3.0	>1.2	<3.0	<1.2
70- and three 34-m	8.2	3.5	>8,2	>3.5	<8.2	<3.5
70- and two 34-m	8.5	4.0	>8.5	>4.0	<8.5	<4.0
70- and one 34-m	10	4.5	>10	>4.5	<10	<4.5

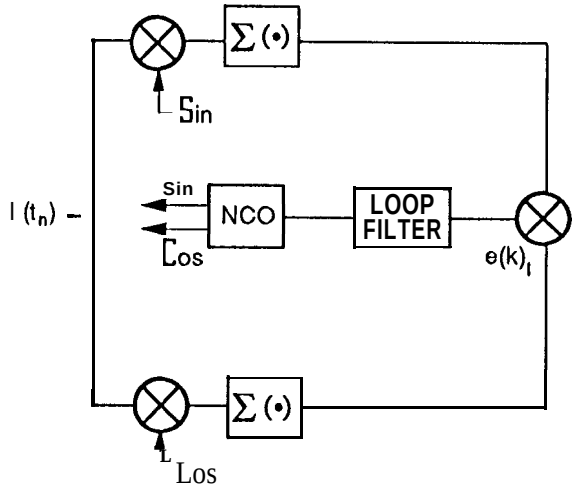

Figure A.1 The unmodified Subcarrier Loop

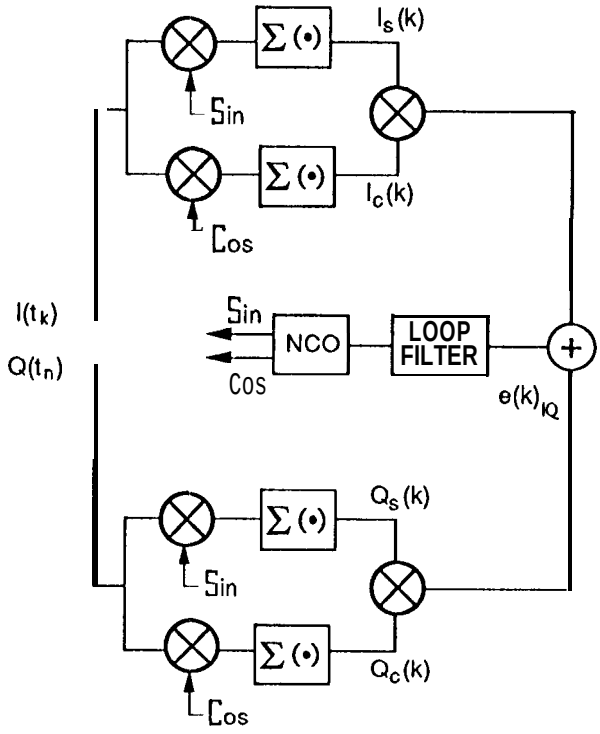

Figure A.2 The modified Subcarrier Loop

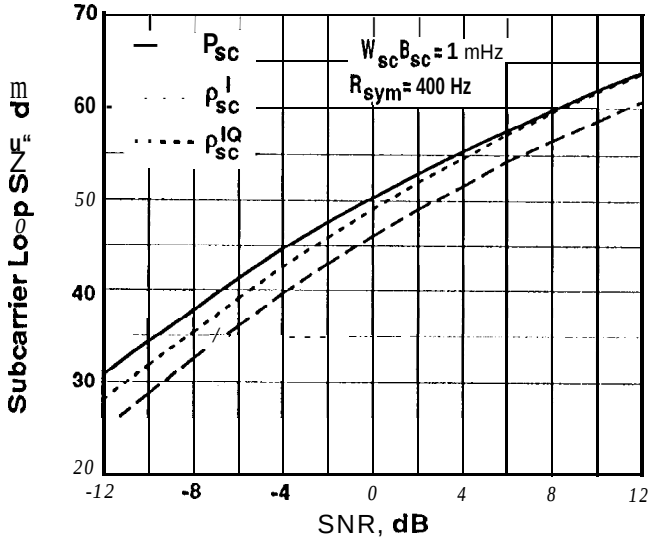

Figure A.3 Subcarrier loop SNR vs symbol SNR

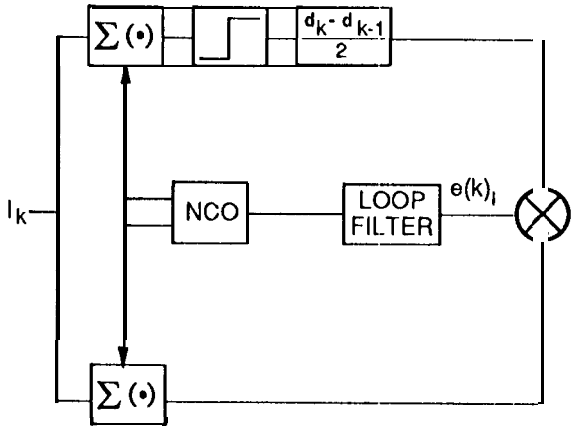

Figure A.4 The unmodified Digital Data Transition Tracking Loop

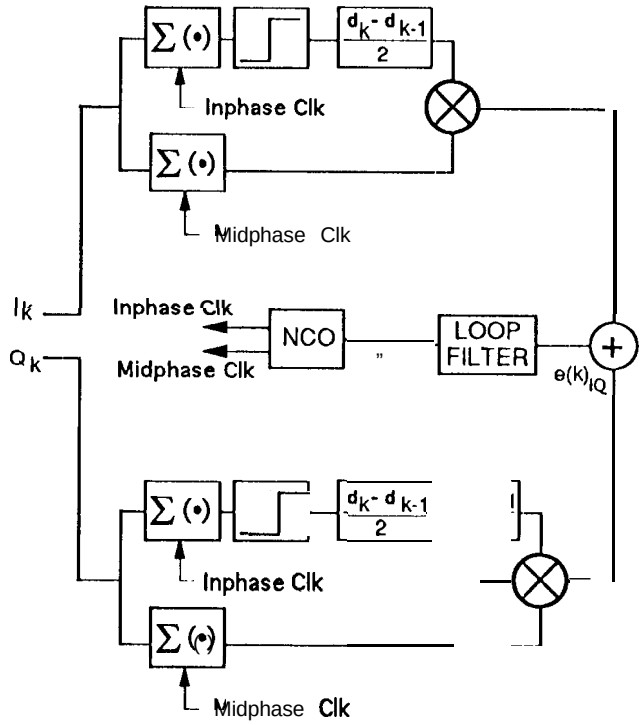

Figure A.5 The modified Digital Data Transition Tracking Loop

Figure A6. DTTL Symbol vs $\frac{K^{I}_{g,sy}}{K_{g,sy}}$ and $\frac{K^{IQ}_{g,sy}}{K_{g,sy}}$

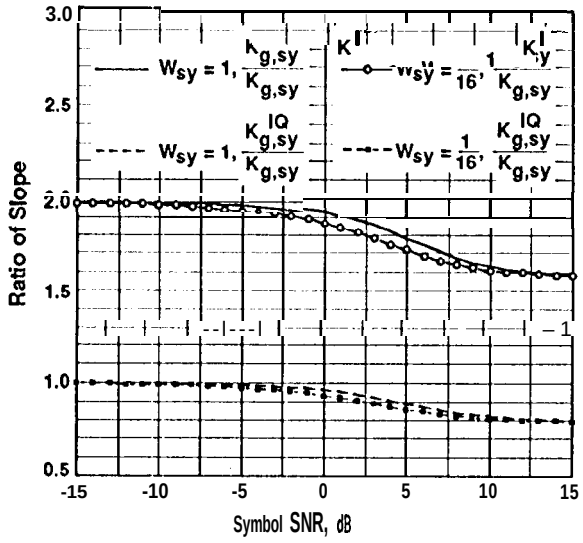

Figure A7. DTTL Symbol SNR vs h(0), $h^{I}(0)$, and $h^{IQ}(0)$ for $W_{SY} = 1$

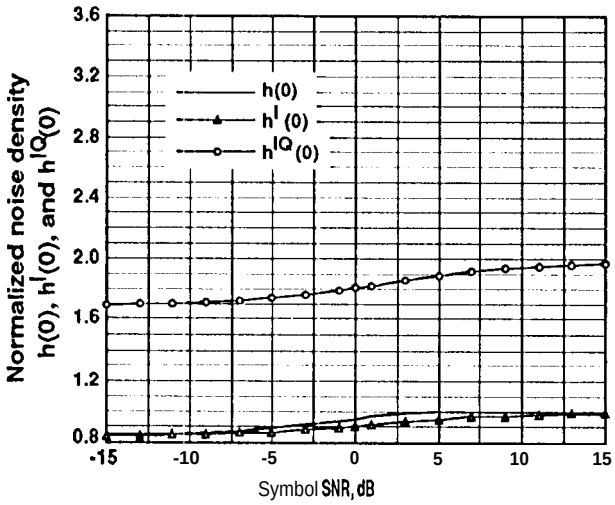

Figure A8. **Symbol loop** SNR vs **symbol SNR**